



Analytical and Computational Model for Predicting the Thermal Performance of PV Cells

Mohamed Gamal Hamdy^{1,*}, Ramadan Bassiouny Mohamed¹,
Hesham Maher¹

¹ Mechanical Power Engineering and Energy Dep., Faculty of Engineering, Minia
University, Minia, Egypt

* Corresponding author(s) E-mail: mohamedgamalhamdy@mu.edu.eg

ARTICLE INFO

Article history:

Received: 23 May 2024

Accepted: 9 December 2024

Online: 1 March 2025

Keywords:

Solar energy,

PV cells,

Analytical solution,

CFD model,

Temperature distribution

ABSTRACT

The photovoltaic, PV, cell is an emerging promising technology used to convert light energy into electrical energy. As fulfilling this function, the cell temperature increases and negatively affects its electrical efficiency. Accurate prediction of the temperature distribution through the PV cell is essential to evaluate its electrical performance. Therefore, the main aim of the present study is to develop a one-dimensional transient analytical model as well as a computational model, using Ansys CFD program to analyze the cell thermal behavior by predicting the temperature distribution through the cell layers at different solar intensity values.

The results insured that operating the PV cell at locations of high solar intensities could negatively affect its performance due to its surface temperature increase. Increasing the solar intensity from 100 to 700 W/m² results in increasing the PV cell average temperature by about 48 % while decreasing the PV electrical efficiency by about 14 %. Hence, cooling techniques of the cell are very necessary to reduce its surface temperature; and accordingly enhance its electrical efficiency. Compared to the no cooling case, increasing the convective heat transfer coefficient at the lower surface of the cell enhances the cell temperature reduction by almost 23%.

1. Introduction

The world has been progressively paying attention to maximize the use of solar energy as a renewable, clean, and economic source in many different applications. These applications are the solar heaters, photovoltaic, PV, module, and hybrid photovoltaic thermal, PVT, systems. The solar heaters benefit from the solar energy intensity variation to efficiently be used in either heating air or water for practical use based on solar collectors of different designs. On the other side, PV cell technology has been recently used to generate electricity based on light energy. For double benefits, a hybrid system to both generate electricity and heat fluids is known as PV/T system.

Solar panels are modules installed using solar cells units. The PV cell is made of crystalline silicon sheets sandwiched between ethylene vinyl acetate "EVA" layers on the front and back typically covered with a glass plate on the front side and mounted in an aluminum frame. The glass allows the solar rays to transmit through and be absorbed by the PV cell. The bottom layer of the cell is made of a substance known as Tedlar. It guarantees that the panel is electrically insulated and protects the cells from environmental damage [1]. Not all the incident light reaches the PV cells due to the properties of the PV panel's layered construction. Therefore, a significant amount of the light transmitted is not converted into electric current [2].

Despite the technological advancements in cell manufacturing, the commercially available solar cells are reported to have efficiencies in the range of only 5-20% which means that most of

the incident radiation is eventually transferred into heat. Consequently, the cell surface temperature increases. Every degree increases in cell surface temperature results in a drop in the cell efficiency at a rate of 0.4–0.65% [3–5]. This increase in cell temperature is the reason of having less electric power than rated capacity, even at higher solar intensity levels.

Previous studies were carried out experimentally, analytically, and computationally. Some had adopted assumptions to be able to obtain an analytical solution such as one-dimensional model, ignoring the radiation losses, setting the sky temperature equal to the ambient temperature, and neglecting the heat absorbed in the glass layer. Also, researchers developed numerical models to analyze the thermal performance of solar cells. Kant et al [6] developed a finite element-based heat transfer model to track the temperature change through a solar panel based on thermal energy balance of the PV module. Similarly, Lee Y and Tay A [7] numerically reported that although the temperature distribution is considered uniform throughout the cell, the closest zone to the frame exhibits 5 °C variation in temperature across each cell. The cell maximum temperature is 66.0 °C corresponding to a solar intensity of 1000 W/m².

A 3D finite element model for polycrystalline silicon photovoltaic modules was developed by Zhou J. et al [8]. The model investigated the effect of various back sheets on the temperature distribution of the module. The results indicated that, under standard test conditions, the solar cell in the module had the highest temperature of 52°C for an ambient temperature of 25°C.

The highest module temperature increased approximately linearly with a change rate of 0.82 K/mm when the thickness of the tedlar back sheet increased from 0.10 mm to 0.70 mm; however, in case of back sheets made of aluminum alloy or tempered glass, a lower temperature within the module was maintained. Sarhaddi F et al [9] numerically investigated the thermal and electrical performance of a solar photovoltaic thermal (PV/T) air collector. The results concluded that the electrical efficiency changes slightly as the inlet air temperature rises from 300 to 315 K, but the thermal and overall energy efficiencies fall by around 8% and 8.6%, respectively. Thermal efficiency and overall energy efficiency are found to rise by roughly 44.5 and 41%, respectively, as inlet air velocity increases from 0 to 10 m/s. Electrical efficiency, on the other hand, varies slightly depending on the inlet air velocity. As wind speed increases from 0 to 10 m/s, overall energy efficiency and thermal efficiency fall by approximately 10% and 14%, respectively. Conversely, as wind speed increases, electrical efficiency rises about 1.5%. When solar radiation intensity is at its optimal level of 700 W/m²—a figure determined by design characteristics and climate—both overall energy efficiency and electrical efficiency rise by approximately 11.4% and 4.5%, respectively. Conversely, there is a minor (~18%) decrease in the thermal efficiency in response to changes in solar radiation intensity.

Previous studies presented different approaches of analyzing solar cells thermal behavior either computationally or analytically. Alternatively, the present study aims to present a transient one-dimensional mathematical model to solve for the cell temperature variation under different operation conditions and compare the results with computational ones using Ansys CFD program considering the effect of convective heat transfer coefficient at the lower surface of the cell.

2. Analytical model for the PV cell

The aim is to predict the temperature distribution through the different layers of the PV cell shown in Figure 1: the glass cover, the upper EVA, the PV cell, the bottom EVA, and the tedlar.

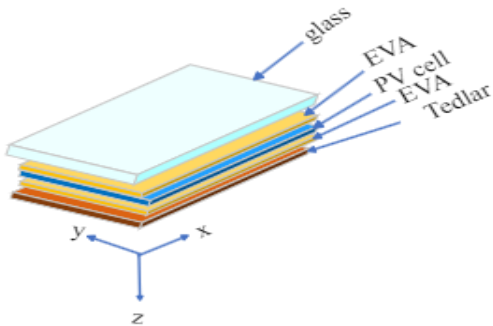


Figure 1: A configuration of the PV cell and its layers

Therefore, a mathematical model with some assumptions has been developed and validated with a numerical solution. The aim of carrying this is to present an analytical solution that can help the designer to predict the maximum average temperature across the PV cell. This would help seeking the proper cooling technique. The model solves one-dimensional transient heat conduction with heat generation. The governing equation is written as:

$$\frac{\partial^2 T}{\partial z^2} + \frac{\dot{q}}{k} = \frac{1}{\alpha} \frac{\partial T}{\partial t} \quad (1)$$

where, k is the layer thermal conductivity, α is the diffusivity, \dot{q} is the heat generation (W/m³), and t is the time. The problem is classified as nonhomogeneous problem due to the heat generation term, \dot{q}/k . Due to this nonhomogeneity, the problem is solved through partial solutions as described below. The partial solution converts the problem into homogenous one as a part of the original problem. Therefore, the problem is solved as a steady-state problem that satisfy the boundary conditions but not the initial conditions. Knowing the steady-state solution forms the general solution as follows:

$$T(z, t) = \bar{T}(z) + v(z, t) \quad (2)$$

where $\bar{T}(z)$ is the steady-state solution. The auxiliary conditions are as follows:

$$T(0, t) = T_u, \quad T(z_l, t) = T_B, \quad T(z, 0) = T_i$$

where, z_l is the layer thickness that varies with layer type.

$$\frac{\partial^2 T}{\partial z^2} + \frac{\dot{q}}{k} = 0 \quad (3)$$

Solving this 2nd order DE considering the boundary conditions gives:

$$\bar{T}(z) = \frac{-\dot{q}}{2k} z^2 + \left(\frac{\dot{q} z_l}{2k} + \frac{\tau l}{k} \right) z + T_u \quad (4)$$

Using the solution in (4) substitute into (2), and carry this into (1) results in:

$$\frac{\partial^2 v}{\partial z^2} = \frac{1}{\alpha} \frac{\partial v}{\partial t} \quad (5)$$

Along with the following homogenous boundary conditions:

$$v(z, t) = T(z, t) - \bar{T}(z)$$

$$v(0, t) = T(0, t) - \bar{T}(0) = 0$$

$$v(z_l, t) = T(z_l, t) - \bar{T}(z_l) = 0$$

and initial condition as:

$$v(z, 0) = T(z, 0) - \bar{T}(z) = \frac{\dot{q}}{2k} z^2 - \left(\frac{\dot{q} z_l}{2k} - \frac{\tau l}{k} \right) z + (T_i - T_u) \quad (6)$$

Using the method of separation of variables assuming $v(z, t) = Z(z) \cdot \theta(t)$

Substitution in equation (5) results in the following equation:

$$\frac{1}{Z} \frac{d^2 Z}{dz^2} = \frac{1}{\alpha \theta} \frac{d\theta}{dt} \quad (7)$$

$$\text{with } Z(0) = 0, \quad Z(z_l) = 0$$

Solving two ordinary differential equations from (7) results in:

$$Z(z) = c_1 \sin \lambda z + c_2 \cos \lambda z, \quad \text{and} \quad \theta(t) = c_3 e^{-\alpha \lambda^2 t}, \quad \text{then}$$

$$v(z, t) = c_3 e^{-\alpha \lambda^2 t} (c_1 \sin \lambda z + c_2 \cos \lambda z)$$

$$= (c_4 \sin \lambda z + c_5 \cos \lambda z) e^{-\alpha \lambda^2 t}$$

where, λ is known as the eigenvalue and defined as $\frac{n\pi}{z_l}$.

Carrying algebraic manipulation results in the following:

$$v(z_l, t) = \sum_{n=1}^{\infty} c_n \sin \lambda_n z e^{-\alpha \lambda^2 t} \quad (8)$$

The initial condition is now brought to the solution, then:

$$v(z, 0) = \sum_{n=1}^{\infty} c_n \sin \frac{n\pi}{z_l} z$$

The coefficient is written in the form of a Fourier series in the value of c_n in the following form:

According to the orthogonality of functions led to:

$$\int_0^{z_l} v(z, 0) \sin \lambda_m z dz = \frac{z_l}{2} \sum_{n=1}^{\infty} c_n$$

$$\text{Then; } c_n = \frac{2}{z_l} \int_0^{z_l} v(z, 0) \sin \frac{n\pi}{z_l} z dz$$

$$c_n = \left[\frac{2(T_i - T_u)}{n\pi} - \frac{2\dot{q} z_l^2}{n^3 \pi^3 k} \right] + \left[\frac{-2(T_i - T_u)}{n\pi} - (n^2 \pi^2 - 2) \frac{\dot{q} z_l^2}{n^3 \pi^3 k} - \left(\frac{\dot{q} z_l^2}{n\pi k} + \frac{2\tau I z_l}{n\pi k} \right) \right] \cos n\pi$$

$$c_n = A + B \cos n\pi$$

$$v(z, t) = \sum_{n=1}^{\infty} c_n \sin \lambda_n z e^{-\alpha \lambda_n^2 t}$$

Since $v(z, 0)$ is known in (6) and recall orthogonality property to obtain the coefficient C_n , this results in the final solution:

$$T(z, t) = T_u + \frac{\dot{q} z}{2k_l} (z - z_l) + \frac{\tau I}{k} z + \sum_{n=1}^{\infty} (A + B \cos n\pi) \sin \lambda_n z e^{-\alpha \lambda_n^2 t} \quad (9)$$

$$\text{where, } A = \frac{2(T_i - T_u)}{n\pi} - \frac{2\dot{q} z_g^2}{n^3 \pi^3 k},$$

$$B = \frac{-2(T_i - T_u)}{n\pi} - (n^2 \pi^2 - 2) \frac{\dot{q} z_g^2}{n^3 \pi^3 k} - \left(\frac{\dot{q} z_g^2}{n\pi k} + \frac{2\tau I z_g}{n\pi k} \right)$$

The heat generation in the PV cell, as a result of electricity generation is related to its electrical efficiency as:

$$\dot{q}_{PV} = \frac{\alpha_{PV} \tau_g I (1 - \eta_{PV})}{z_{PV}} \text{ and}$$

$$\eta_{PV} = \eta_{PV,ref} [1 - \beta_{ref} (T_{PV,cell} - T_{ref})]$$

For most crystalline silicon PV cells, β_{ref} is the reference temperature coefficient of the PV cells and has a reasonable value of 0.005 K^{-1} ; where the manufacturer provides a reference electrical efficiency of 13.5 %, denoted by $\eta_{PV,ref}$. T_{ref} is the temperature reference (298.15 K) [10].

3. Numerical model for PV cell

A two-dimensional computational domain that simulates the physical domain of the PV cell, is shown in Figure 2 Ansys Fluent 2020 was used to generate grids and obtain solution. The photovoltaic panel is composed of five layers: glass, two ethylene-vinyl acetate (EVA), solar silicon cell, and tedlar whose physical and optical properties are shown in Table 1. The heat diffusion governing equation is discretized using the finite volume method.

In the computational domain, the mesh is refined near the interfaces between layers to capture the proper temperature gradient. The grid independence test has been done as shown on Figure 2 and there is no significant change is noticed.

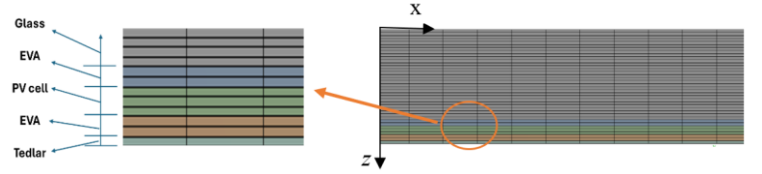


Figure 2: The generated mesh of the PV numerical model

Table 1: Material, physical and optical properties of each PV layer [11]

Layer	Thickn ess z (mm)	Thermal conductivity k (W/m K)	Densit y ρ (kg/m ³)	Specific heat capacity, C (J/kg k)	τ	α
Glass	3	1.8	3000	500	0.9	0.1
EVA	0.2	0.35	960	2090	1	0
PV Cells	0.3	148	2330	677	0	0.85
Tedlar	0.1	0.2	1200	1250	-	-

The energy equation is solved for the domain of different layers with setting boundary conditions of heat flux at the upper surface with no convection while the convection at the lower surface of the cell. Figure. 3 shows the boundary conditions for the whole cell.

The assumptions were adopted in the model:

- Steady conduction over a certain solar intensity and no reflection.
- The sky temperature is regarded as the black body temperature.
- A uniform distribution of solar radiation.
- No dust on the glass.
- All material's characteristics are isotropic and temperature independent.
- Thermal contact resistance is negligible, and the end sides are adiabatic.
- Optical properties are independent of solar intensity.
- The wind direction is parallel to module from surface.
- EVA transmittivity is one, PV efficiency is 15%, and whole cell is exposed to the same ambient temperature.

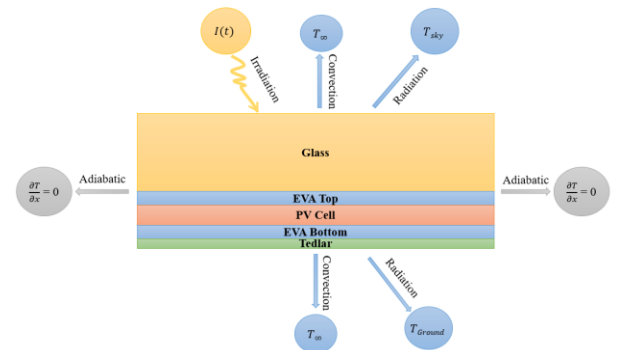


Figure 3: Schematic diagram for the PV cell and accompanied boundary conditions

The solution must be grid independent. Therefore, four grid sizes configurations were applied, and the cell average temperature was plotted versus the grid number. In Figure 4, the solution was based on solar intensity 970 W/m², ambient temperature 42 °C and wind speed of 3 m/s. The values varied till there no significant variation was noticed at grid configuration of 250x80.

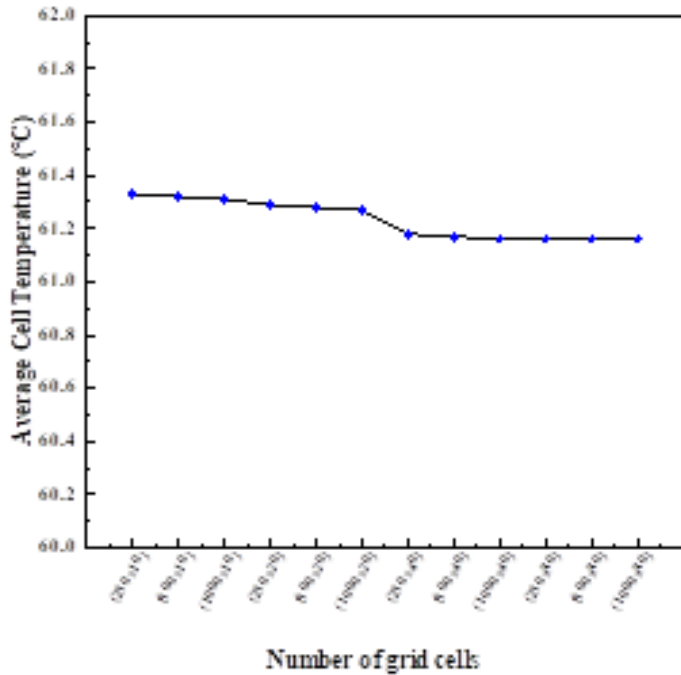


Figure 4 Numerical mesh sensitivity of the average temperature of the PV cell

4. Model Validation

The theoretical results obtained through the developed model at wind speed 3 m/s are validated using published results from Duffie and Beckman [12] and Aly S. et al [10]. The compared results are summarized in Table 2. The results showed good agreement with reported results in [12] and [10] with a daily reasonable average error of 4% and 5%, respectively at the same wind speed.

Table 2: Model validation

Time	T _{amb} (°C)	I (W/m ²)	T _{cell} (°C)	T [10] (°C)	Erro r %	T [12] (°C)	Erro r %
8 am	36	600	52	46.1	12.7	46.41	12
10 am	41	900	58.63	58.3	0.56	56.6	3.5
12 noon	42	970	59.46	61.5	3.31	58.8	1.1
2 pm	42.5	700	52.53	55.5	5.35	52.44	0.17
4 pm	41	340	47.8	46.4	3.01	45.83	4.2

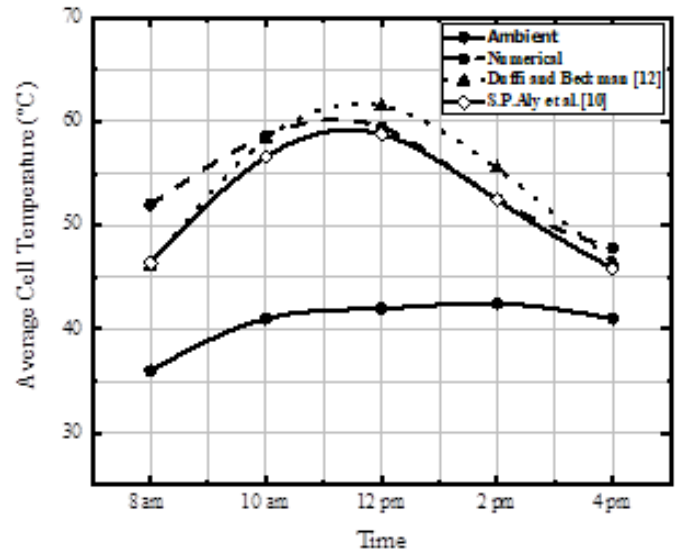


Figure 5: Average Temperature of PV numerical model in comparison with different models

5. Results and Discussion

In the model, the temperature distribution across each layer of the PV module was predicted along the thickness direction (y direction) to capture the PV module's temperature change trend when sunlight enters via the top glass, EVA, and PV cell up till the tedlar sheet, as displayed in Figure 6. The results showed that the maximum temperature difference between cell temperature and ambient temperature reaches 20 °C at the highest solar intensity. When the sunlight reached the module from the top glass layer, the module's temperature started to increase and reached its peak at the PV cell layer due to layer's high absorptivity. After converting part of the transmitted energy into electrical energy, the remaining energy is conducted to the front and back surfaces of the cell in the form of heat then dissipated to the surrounding ambient air.

The cell's front surface temperature is lower than its back temperature as in Figure 6. This can be attributed to the less resistance in the direction to the tedlar layer at the back surface compared to the glass layer resistance at the upper surface of the PV cell. As a result, the temperature difference between the PV cell layer and the Tedlar layer was about 1°C.

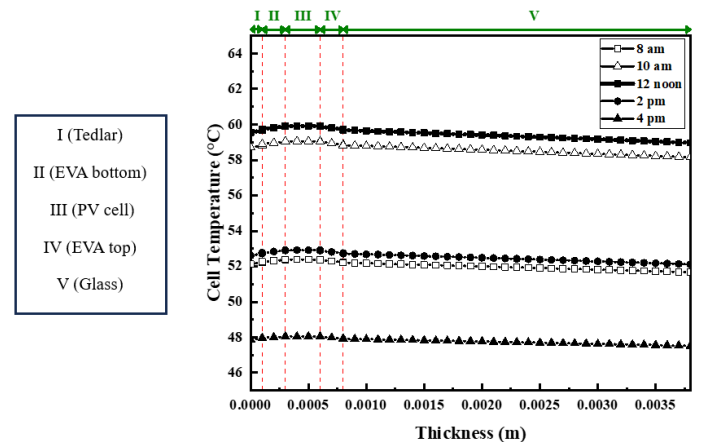


Figure 6: PV Cell temperature distribution through the different layers at different times

Figure 7 indicates the temperature variation of different layers in a contour form with color legend. The temperature gradient displays the regions of high temperature at the PV cell, where electricity is generated. The average temperature for every layer can be estimated.

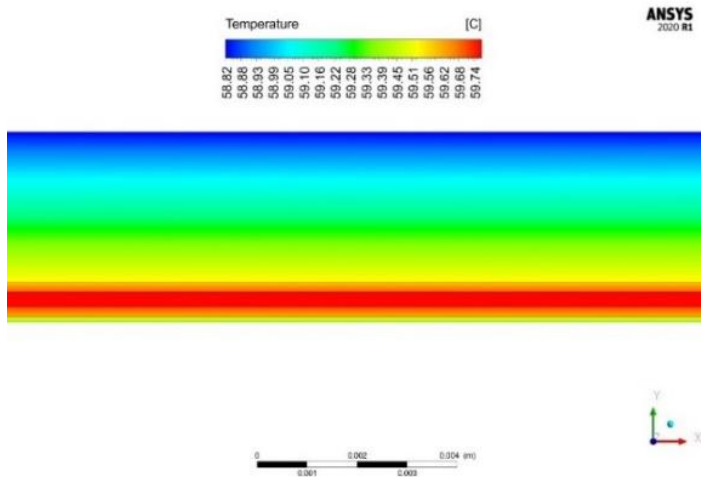


Figure 7: Temperature contour of the longitude section of the PV module at noon time

The performance of the PV module is location dependent. Hence, the installation of such module performs differently according to weather conditions. The ambient temperature, cell average temperature, and solar intensity variations over daytime for five cities in Egypt (Alexandria, Cairo, Minia, Aswan and Red Sea) are shown in Fig. 8 for the month of July. As seen in the figure, the city of Aswan has the highest solar intensity by 925 W/m², ambient temperature around 43°C and as a result is the cell temperature approximately 57.5 °C while the lowest was in Alexandria.

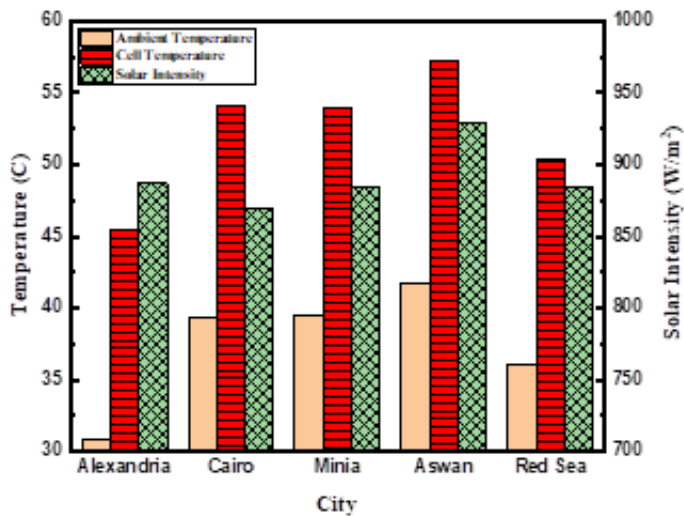


Figure 8: Variation of cell temperature with place of installation

In order to judge the rationality of the obtained temperature distribution, a comparison was held between the analytical and numerical average cell temperature across a function of thickness in case of no convection at the bottom surface, Fig. 9. As shown in the figure, still the temperature is high at the PV cell layer due to

its high absorptivity then it decreases towards the other layers because these Layers like glass and EVA having a very high transmissivity to sunlight. Similar trends are noticed with temperature increase as solar intensity increases.

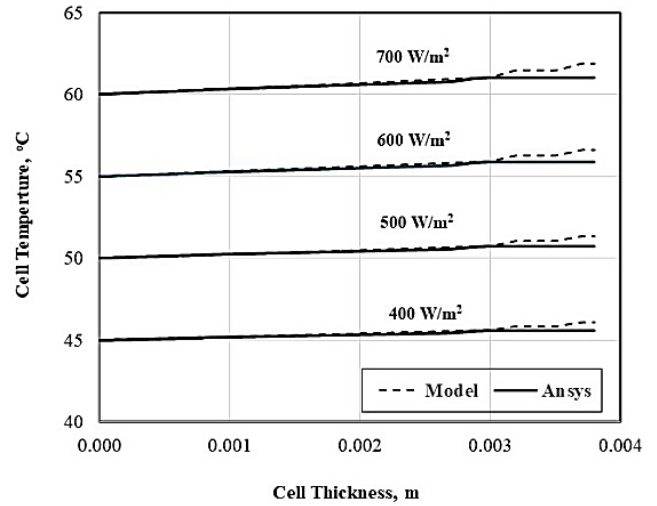


Figure 9: Temperature distribution across the PV cell in case of no convection at the bottom surface

The results showed an increase in the cell temperature with the increase in solar intensity. In contrast, the cell efficiency decreases as shown in Fig.10. The cell average temperature ranges from 45 to 60 °C, and the cell electrical power is from 43 to 71 W/m², while the PV electrical efficiency is from 0.125 to 0.145. Increasing the solar intensity from 400 to 700 W/m² results in increasing the PV cell average temperature and electrical power by about 34 % and 62% respectively while decreasing the PV electrical efficiency by about 7.35 % when the air temperature varied from 45 °C to 60 °C. Although there is the electrical power as the solar intensity increases, however this increase is less in magnitude compared to the increase of solar intensity. Hence, in order to preserve cell conversion efficiency, a cooling technique should be adopted at the bottom of the cell panel.

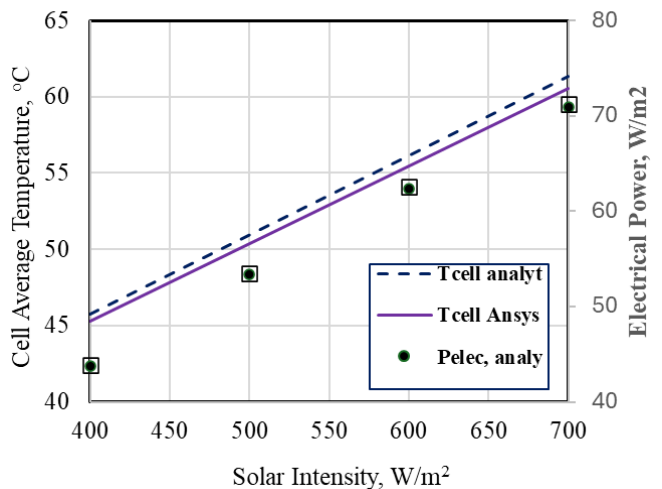


Figure 10: Cell average temperature and cell efficiency at different solar intensity

Figure 11 illustrates the effect of varying convective heat transfer coefficient at the bottom surface of the PV cell. As shown in the figure, the highest cell temperature is with no cooling at the bottom surface, 66 °C, that is started to decrease as convective heat transfer was considered. As the convective heat transfer coefficient reached 10 W/m² K, the cell cooled by 6 °C. Further increase in the convective heat transfer coefficient resulted in a further decrease in the cell temperature. Almost a decrease of almost 23% was achieved by increasing the convection heat transfer coefficient from 10 to 50 W/m² K.

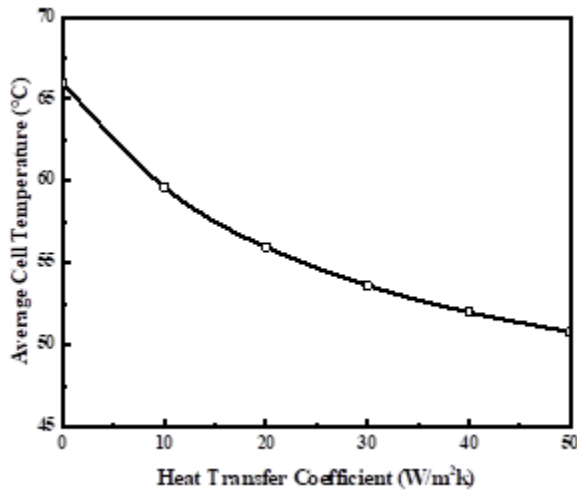


Figure 11: Effect of considering convective heat transfer coefficient at the bottom of the cell-on-cell temperature

6. Conclusions

The study tried to contribute to the PV cell analysis helping to model cell cooling based on understanding the cell thermal behavior with no cooling. Therefore, this is a mathematical analysis for the governing equation for unsteady behavior as the solar intensity and air temperature varies over the day. Also, the effect of layer different thicknesses was considered. Some conclusions can be drawn out of the results as follows:

1. In order to validate the mathematical predication, a comparison with a computational analysis showed a reasonable agreement in terms of cell average temperature variation and produced electrical power.
2. The highest cell temperature is noticed at the PV layer that increases by about 43 % as the solar intensity increases from 400 to 700 W/m² as well as the electrical power increases by about 62 %, while the air temperature varied from 45 °C to 60 °C resulting in electrical efficiency decrease by about 7.35 %.
3. Increasing the convective heat transfer coefficient around the cell by almost five times the natural free convection resulted in a reduction in the cell average temperature by almost 20%, which accordingly enhances the cell output power.

Conflict of Interest

The authors declare no conflict of interest.

Nomenclature

c_p	specific heat capacity (J/kg k)
h	convective heat transfer coefficient (W/m ² k)
I	solar radiation (W/m ²)
K	thermal conductivity (W/m k)
q	heat generation (W/m ³)
t	time (s)
T	Temperature (°C)
V	speed (m/s)
Z	layer thickness (m)

Greek symbols

A	absorptivity
β	reference Temperature coefficient
ε	emissivity
η	efficiency
ρ	density, (kg/m ³)
τ	transmittivity

Subscripts

amb	Ambient
B	Bottom
g	glass
i	initial
l	layer
Ref	reference
u	upper

References

- [1] Solar Panel Manufacturing - AESOLAR, (n.d.). <https://ae-solar.com/solar-panel-manufacturing/> (accessed June 27, 2023).
- [2] F.H. Alharbi, S. Kais, Theoretical limits of photovoltaics efficiency and possible improvements by intuitive approaches learned from photosynthesis and quantum coherence, *Renewable and Sustainable Energy Reviews* 43 (2015) 1073–1089. <https://doi.org/10.1016/j.rser.2014.11.101>.
- [3] A. Nahar, M. Hasanuzzaman, N.A. Rahim, Numerical and experimental investigation on the performance of a photovoltaic thermal collector with parallel plate flow channel under different operating conditions in Malaysia, *Solar Energy* 144 (2017) 517–528. <https://doi.org/10.1016/j.solener.2017.01.041>.
- [4] J. Siecker, K. Kusakana, B.P. Numbi, A review of solar photovoltaic systems cooling technologies, *Renewable and Sustainable Energy Reviews* 79 (2017) 192–203. <https://doi.org/10.1016/j.rser.2017.05.053>.
- [5] A.R. Abdulmunem, P.M. Samin, H.A. Rahman, H.A. Hussien, H. Ghazali, A novel thermal regulation method for photovoltaic panels using porous metals filled with phase change material and nanoparticle additives, *J Energy Storage* 39 (2021). <https://doi.org/10.1016/j.est.2021.102621>.
- [6] K. Kant, A. Shukla, A. Sharma, P.H. Biwole, Thermal response of polycrystalline silicon photovoltaic panels: Numerical simulation and experimental study, *Solar Energy* 134 (2016) 147–155. <https://doi.org/10.1016/j.solener.2016.05.002>.
- [7] Y. Lee, A.A.O. Tay, Finite element thermal analysis of a solar photovoltaic module, *in: Energy Procedia*, 2012: pp. 413–420. <https://doi.org/10.1016/j.egypro.2012.02.050>.
- [8] J. cheng Zhou, Z. Zhang, H. jian Liu, Q. Yi, Temperature distribution and back sheet role of polycrystalline silicon photovoltaic modules, *Appl Therm*

- [9] F. Sarhaddi, S. Farahat, H. Ajam, A. Behzadmehr, M. Mahdavi Adeli, An improved thermal and electrical model for a solar photovoltaic thermal (PV/T) air collector, *Appl Energy* 87 (2010) 2328–2339. <https://doi.org/10.1016/j.apenergy.2010.01.001>.
- [10] S.P. Aly, S. Ahzi, N. Barth, A. Abdallah, Using energy balance method to study the thermal behavior of PV panels under time-varying field conditions, *Energy Convers Manag* 175 (2018) 246–262. <https://doi.org/10.1016/j.enconman.2018.09.007>.
- [11] S. Armstrong, W.G. Hurley, A thermal model for photovoltaic panels under varying atmospheric conditions, *Appl Therm Eng* 30 (2010) 1488–1495. <https://doi.org/10.1016/j.applthermaleng.2010.03.012>.
- [12] J.A. Duffie, W.A. Beckman, *Solar engineering of thermal processes*, n.d.